HHS Public Access

Author manuscript

Reprod Toxicol. Author manuscript; available in PMC 2022 November 17.

Published in final edited form as:

Reprod Toxicol. 2022 August ; 111: 184–193. doi:10.1016/j.reprotox.2022.06.002.

Toward a digital analysis of environmental impacts on rodent mammary gland density during critical developmental windows

Alina M. Hamilton[a], **Linnea T. Olsson**[b], **Bentley R. Midkiff**[c], **Elena Morozova**[d], **Yanrong Su**[e], **Sandra Z. Haslam**[f], **Laura N. Vandenberg**[g], **Sallie S. Schneider**[h,i], **Julia Santucci-Pereira**[e], **D. Joseph Jerry**[h,j], **Melissa A. Troester**[b,c], **Richard C. Schwartz**[d,*]

[a]Department of Pathology and Laboratory Medicine, School of Medicine, University of North Carolina at Chapel Hill, Chapel Hill, NC, USA

[b]Department of Epidemiology, Gillings School of Public Health, University of North Carolina at Chapel Hill, Chapel Hill, NC, USA

[c]Lineberger Comprehensive Cancer Center, University of North Carolina at Chapel Hill, Chapel Hill, NC, USA

[d]Department of Microbiology and Molecular Genetics, Michigan State University, East Lansing, MI, USA

[e]The Irma H. Russo MD Breast Cancer Research Laboratory, Fox Chase Cancer Center, Temple University Health System, Philadelphia, PA, USA

[f]Department of Physiology, Michigan State University, East Lansing, MI, USA

[g]Department of Environmental Health Sciences, University of Massachusetts, Amherst, MA, USA

[h]Pioneer Valley Life Sciences Institute, Springfield, MA, USA

[i]Department of Surgery, University of Massachusetts Medical School-Baystate, Springfield, MA, USA

[j]Department of Veterinary and Animal Sciences, University of Massachusetts Amherst, Amherst, MA, USA

[*]Correspondence to: Department of Microbiology and Molecular Genetics, Michigan State University, 567 Wilson Road, Room 2209, East Lansing, MI 48824, USA, schwart9@msu.edu (R.C. Schwartz).

Declaration of Competing Interest

The authors declare the following financial interests/personal relationships which may be considered as potential competing interests: Richard C. Schwartz reports financial support was provided by National Institutes of Health. Alina M. Hamiltion reports financial support was provided by National Institutes of Health. Linnea T. Olsson reports financial support was provided by National Institutes of Health. Bentley R. Midkiff reports financial support was provided by National Institutes of Health. Bentley R. Midkiff reports financial support was provided by University Cancer Research Fund - Lineberger Comprehensive Cancer Center. Bentley R. Midkiff reports financial support was provided by North Carolina Biotechnology Center. Elena Morozova reports financial support was provided by National Institutes of Health. Yangrong Su reports financial support was provided by National Institutes of Health. Sandra Z. Haslam reports financial support was provided by National Institutes of Health. Laura N. Vandenberg reports financial support was provided by National Institutes of Health. Sallie S. Schneider reports financial support was provided by National Institutes of Health. Julia Santucci-Pereira reports financial support was provided by National Institutes of Health. D. Joseph Jerry reports financial support was provided by National Institutes of Health. Melissa A. Troester reports financial support was provided by National Institutes of Health.

Appendix A. Supporting information

Supplementary data associated with this article can be found in the online version at doi:10.1016/j.reprotox.2022.06.002.

Abstract

While mammographic breast density is associated with breast cancer risk in humans, there is no comparable surrogate risk measure in mouse and rat mammary glands following various environmental exposures. In the current study, mammary glands from mice and rats subjected to reproductive factors and exposures to environmental chemicals that have been shown to influence mammary gland development and/or susceptibility to mammary tumors were evaluated for histologic density by manual and automated digital methods. Digital histological density detected changes due to hormonal stimuli/reproductive factors (parity), dietary fat, and exposure to environmental chemicals, such as benzophenone-3 and a combination of perfluorooctanoic acid and zeranol. Thus, digital analysis of mammary gland density offers a high throughput method that can provide a highly reproducible means of comparing a measure of histological density across independent experiments, experimental systems, and laboratories. This methodology holds promise for the detection of environmental impacts on mammary gland structure in mice and rats that may be comparable to human breast density, thus potentially allowing comparisons between rodent models and human breast cancer studies.

Keywords

Mammary density; Digital histology; Breast cancer; Parity; High fat diet; Benzophenone-3; Perfluorooctanoic acid; Zeranol

1. Introduction

Rodents provide important models to investigate the influence of environmental chemicals and genetic mechanisms on mammary gland health and disease, and have served as models for understanding breast cancer risk factors in humans. The mammary glands of rats and mice are sensitive to the hormonal factors that drive breast development in humans, and endocrine disrupting chemicals can lead to altered mammary gland development and susceptibility to tumors [1]. Several methods have been used to quantify the effects of exposures to exogenous hormones and endocrine disrupting chemicals. Most often, wholemounts of rodent mammary glands have been used to determine structural features, such as ductal elongation and branching in pubertal animals. A manual method has used unbiased stereology to determine the impact of environmental chemicals on epithelial branching in mammary gland wholemounts [2]. Sholl analysis, originally used to quantify neuronal patterns, was adapted to quantify branching in whole mounts of rat mammary glands using ImageJ software [3]. An alternate approach involved using digital images of mammary glands and circumscribing the ductal regions to estimate the volume of epithelial and stromal regions (i.e., epithelium-free stroma) as a means to determine the mass of tissue and relative density of the epithelial area [4]. Although analyses of whole mounts are effective in evaluating global changes in ductal components, the approach is less sensitive to alterations in other components of mammary glands and are not easily translated to evaluation of human breast tissues.

In contrast, tissue sections stained with hematoxylin and eosin (H&E) can be prepared with tissues from rodent models and human breast tissues, and allow detailed evaluation of

adipose and stromal components of the mammary gland as well as the ductal epithelium. Tissue sections are used routinely for histopathology and diagnosis of breast cancer. Women with premalignant breast lesions, such as atypical ductal hyperplasia and lobular carcinoma in situ, have relative risks of breast cancer that are ~4-fold greater than do women without these microscopic areas of histologic density [5,6, reviewed in 7]. Recent work used analysis of digital images of H&E-stained human breast tissues to quantify changes in epithelial, stromal, and adipose compartments [8]. This method employed algorithms to assess the intensity of staining and features that define these compartments to automate scoring. The digital histologic density scores that were produced were associated with measures of mammographic breast density. In particular, stromal features had a significant contribution to mammographic density and varied in association with several human risk factors [9]. This raises the question of whether the stromal features of mammary glands in rodent models of breast cancer are also predictive of risk to develop mammary tumors and whether pre-neoplastic alterations of the mammary stroma that might support mammary tumorigenesis can be identified. Digital histologic density provides a tool developed on human breast tissues that can be used to evaluate rodent mammary tissues and identify cross-species effects of chemical and hormonal exposures that are related to breast cancer risk.

A variety of reproductive factors and exposures to environmental chemicals have been shown to influence mammary gland development and/or susceptibility to mammary tumors. A full-term pregnancy imposes changes in the structure of the human breast that increase the presence of complex lobular structures indicative of a more differentiated state [reviewed in 10]. This is associated with an overall reduction of breast cancer risk among parous women [11,12]. Similarly, a full-term pregnancy reduced the incidence of carcinogen-induced mammary tumors in rats [13,14] and in mice with heterozygous mutations in the *Trp53* gene [15]. Environmental chemicals have also been shown to disrupt endocrine signaling pathways, altering both the development of the mammary gland as well as modifying the incidence of mammary tumors [reviewed in 16]. For example, benzophenone-3 (BP-3; also referred to as oxybenzone), a common ingredient in sunscreens that is prevalent in human urine samples in the United States [17, reviewed in 18] has been shown to alter mammary gland development [19,20]. The level of dietary animal fat also alters mammary gland development [21] and promotes mammary tumorigenesis [22–25]. A high fat diet interacts with BP-3 treatment to promote epithelial mammary tumors in *Trp53-null* mammary transplants [26]. Perfluorooctanoic acid (PFOA), an environmental chemical commonly used as a surfactant, affects ovarian function [27], and inhibits mammary gland development in mice [28–31]. Zeranol, an endocrine disrupting chemical used as an anabolic growth promoter for meat production and also found in *Fusarium* contaminated grain, has estrogen receptor binding activity [reviewed in 31]. Prepubertal treatment of rats with zeranol negatively affects ovarian structure and function without promoting mammary tumorigenesis [32].

In the studies reported here, rodent models for mammary tumorigenesis were subjected to treatments that modify the incidence of mammary tumors in rodents [22–26,33]. The tissues from mice and rats were then evaluated for histologic density by manual and automated digital methods. These histologic density methods were successfully applied to both mouse and rat mammary tissues. Our results suggest that digital histologic density offers a higher

throughput method to evaluate effects of reproductive factors (e.g., parity), diet (e.g., animal fat), and exposures to environmental chemicals (e.g., BP-3, PFOA, zeranol) that affect susceptibility to mammary tumors. These methods can provide a highly reproducible means of comparing a measure of histological density across independent experiments, experimental systems, and laboratories.

2. Methods

The diversity of preclinical models used in environmental studies can make direct comparison to human studies and between labs challenging, and a method that is robust and that can be applied across multiple settings has value for improving data integration. Thus, three rodent model exposed to regimens with known impact on mammary tissue composition were selected from separate laboratories to develop a robust digital histological analysis pipeline and are described as follows. For each model, sample sizes of either 5 or 6 were chosen to comprise groups of comparable size.

2.1. Parity and BP-3 in Mice

Six- to 8-week-old female BALB/cMed mice were mated with males and housed in polysulfone cages with food (LabDiet Chow 5058; LabDiet, St. Louis, MO) and water provided ad libitum as described [19]. The mice were exposed to either vehicle (tocopherol-stripped corn oil; n = 5) or BP-3 (oxybenzone, or 2-Hydroxy-4-methoxybenzophenone, CAS No. 131–57–7; n = 5) throughout pregnancy and lactation (~6 weeks total). A separate group of age-matched nulliparous females (n = 5) was administered vehicle as well. The corn oil intake was 1 μl/g body weight/day delivered orally. The dose of BP-3 selected represents the no-observed adverse-effect level (NOAEL, 3,000 μg/kg/d). After 21 days of lactation, BP-3 treatment ceased, and pups were removed allowing dams to undergo mammary involution. At 5 weeks postweaning, the parous females and age-matched nulliparous females were euthanized via CO_2 inhalation and the 4th inguinal mammary glands were removed and fixed in neutral-buffered formalin (10 %) overnight, transferred to 70 % ethanol, and then processed for paraffin embedding. Longitudinal tissue sections (5 μm) were stained with H&E or Masson's trichrome. Mice were maintained at the University of Massachusetts Amherst, Amherst Animal Facility, in temperature- and light-controlled conditions (12 h light, 12 h dark). All experimental procedures were approved by the University of Massachusetts Institutional Animal Care and Use Committee.

2.2. Dietary Fat and BP-3 in Mice

In order to examine the interaction between dietary fat and BP-3 in mammary tumorigenesis, a *Trp53-null* transplantation system was used in BALB/c mice. *Trp53-null* mammary tissue provided a measurable rate of tumor incidence [34] in which to observe treatment effects, while BALB/c mice are obesity resistant [35], allowing dissociation of the effects of dietary fat in itself from obesity, BALB/c *Trp53* + /− breeding mice were obtained from Dr. D. Joseph Jerry (University of Massachusetts, Amherst MA), and *Trp53-null* mice were generated as described [34]. The female *Trp53-null* tissue donor mice were maintained on standard laboratory rodent diet (LabDiet 5001; LabDiet, St. Louis, MO) before mammary

gland collection at eight weeks of age. Wild-type recipient female BALB/c mice were purchased from Charles River (Portage, MI) at 3 weeks of age.

For experiments assessing the effects of BP-3 and diet, female *Trp53-null* transplanted mice were randomly assigned into four diet groups (see below) and LFD was the control diet for all statistical comparisons. Food and water were provided ad libitum. Mice were housed in a standard laboratory housing environment with a 12:12 h light–dark cycle, at 20–24 °C with 40–50 % relative humidity. All animal experimentation was conducted in accord with accepted standards of humane animal care under guidelines approved by the All University Committee on Animal Use and Care at Michigan State University (AUF #07/17–128–00).

Trp53-null transplanted mice were generated as follows. Fragments of donor mammary epithelium were collected from female BALB/c *Trp53-null* mice at 8 weeks of age and transplanted into the cleared inguinal mammary fat pads of 3-week-old female wild type BALB/c mice as previously described [36,37]. To minimize donor bias from secondary genetic alterations, mammary duct fragments from 4 donor mice were transplanted to recipient mice in each diet group in equal distribution. Body weights and food consumption were monitored weekly. Mice were euthanized at 13 weeks of age prior to the appearance of lesions or tumors. Inguinal mammary glands were formalin-fixed, paraffin embedded, and sectioned longitudinally for H&E analysis. Mammary glands that had no epithelium present were excluded from this analysis.

Low fat diet (LFD) (D11012202; 10 % kcal fat) and high fat diet (HFD) (D11012204; 60 % kcal fat) were purchased from Research Diets (New Brunswick, NJ). For the continuous LFD (n = 5) and HFD (n = 5) groups, the diet was initiated after transplantation at 3 weeks of age and maintained throughout the studies. For the LFD-HFD (n = 5) group, mice were initially fed LFD from 3 weeks until 10 weeks of age, and then switched to HFD thereafter. For the HFD+ BP-3 (n = 5) diet, BP-3 (Spectrum Chemical, New Brunswick, NJ) was compounded into the diet at 0.75 g/kg chow for pubertal animals (3–10 weeks of age) and 1.5 g/kg chow for adult animals; the difference in BP-3 between the diets for pubertal and adult animals was intended to compensate for the differences in food consumption and body weight with age and yielded BP-3 consumption of approximately 70 mg/kg body weight/d. BP-3 consumption was similar between LFD and HFD, and between pubertal and adult animals. BP-3 excretion in the urine voided at euthanasia for mice treated with BP-3 ranged between 1.0 and 6.1 mg/kg body weight with no significant differences between diet. We selected our dosage to yield levels of BP-3 urine excretion similar to values to observed in a small human cohort that was exposed to heavy topical application of a BP-3 containing sunscreen [38], approximately 2.3 mg/kg body weight, assuming an average European adult body weight of 70.8 kg [39]. Considering the rapid excretion of BP-3 in mice [26], it is likely that our dosage generates urine excretion on the same order as that observed in heavily exposed humans. Determination of BP-3 levels in urine was performed by the Division of Laboratory Sciences of the National Center for Environmental Health, Center for Disease Control and Prevention (Atlanta, GA), as reported previously [40].

2.3. PFOA and zeranol in rats

The potential interaction between PFOA and zeranol, two putative endocrine disrupting chemicals, was assessed in Sprague Dawley rats because rat mammary gland morphology and development are relatively similar to those of humans [41] and because Sprague Dawley rats are highly sensitive to DMBA-induced mammary tumorigenesis [42], which was studied in experiments that paralleled those presented here. Sprague Dawley rats (Taconic Biosciences, Inc., Rensselaer, NY) were bred and kept in the Laboratory Animal Facility at Fox Chase Cancer Center. Animal care and use were conducted according to established guidelines approved by Fox Chase Cancer Center's Institutional Animal Care and Use Committee. At 21 days of age, the female offspring were weaned, housed in polypropylene cages with water bottles (polycarbonate/BPA free) in a temperature-controlled room (23 – 25 °C) with 12-hour light/dark cycle, and received irradiated AIN-93 G diet (TD.97 184, Harlan Teklad, Madison, WI) to decrease their exposure to phytoestrogens.

Female rats were administered either sesame oil (control group; n = 6) or a combination of PFOA and zeranol daily from day 21 to day 42 (Monday through Friday) (n = 6) through gavage. For the combined treatment, the animals were exposed to a mixture of 0.01 mg/kg per body weight of PFOA (Sigma-Aldrich, St. Louis, MO; #171 468) and 0.01 mg/kg body weight of zeranol (FUJIFILM Wako Pure Chemical Corporation, Osaka, Japan; #262–1 461) dissolved in sesame oil (Sigma-Aldrich, #S3547).

At day 50, the rats were euthanized, and the 4th and 5th mammary glands were collected, fixed in 10 % neutral buffered formalin at least for 24 h, then processed and embedded in paraffin blocks. Longitudinal paraffin sections at 4 μm thickness were used for H&E staining and evaluation.

2.4. Digital histological analysis pipeline

2.4.1. Slide scanning and annotation—Slides were scanned using either Aperio ScanScope XT or Versa slide scanners (Leica Biosystems), and then stored on Aperio eSlideManager. Aperio ImageScope was used to perform tissue annotation for all three datasets. The same pipeline strategy was used whether the slides were stained with H&E or Masson's trichrome.

Using the negative annotation pen in Aperio ImageScope and as illustrated in Fig. 1, slides were manually annotated to exclude scanning or fixation artifacts such as bubbles or shadows and small regions of tissue that were not relevant to the analysis, such as tissue folds, large blood vessels or nerves. To account for variation in tissue collection and extent of tissue present (including variability in the amount of epithelium and fat pad collected), we used the free-form annotation pen in Aperio ImageScope to manually select analysis area. To standardize across studies, we restricted analyses to the epithelial tree, excluding any non-invaded fat pad.

2.4.2. Classifier development and refinement—We utilized two image analysis platforms to develop classifiers, or computational algorithms, that can classify, partition and

quantify mammary tissue section area into regions of glass, epithelium, stroma, and adipose tissue across all studies: Aperio GENIE and Definiens Tissue Studio Composer.

Briefly, for each study, training regions or "classes" representative of glass, epithelium, stroma, and adipose tissue were manually identified from each set of tissue sections and designated as training regions using Aperio ImageScope. Within these training regions, discrete areas of each of the three tissue types and glass were selected using the free-form annotation tool, designating each tissue type in a separate "annotation layer". These regions were used to build the tissue partitioning classifier. Visual inspection of the tissue partitioning was performed and modifications to the algorithm were made using adjustment parameters based on tissue characteristics like cell/nuclear size or staining coloration and intensity. Iterations of these modifications were conducted until study personnel were satisfied with the accuracy of classification before applying the classification algorithm to all slides or mammary tissue sections within a study.

Note that classifiers were developed in a two tier approach— we refined first within GENIE because of its convenient integration with ImageScope. However, when tissue partitioning using the first platform was unsatisfactory and use of additional adjustment parameters (cell/nuclear size or staining coloration and intensity) were needed, a second algorithm was developed and refined using the Definiens platform, which includes more detailed refinement parameters. Final quantification of tissue type area was performed on one platform for each study. In addition, each study's set of slides should be considered carefully to ensure accurate area measurements. For example, for one study with a higher frequency of red blood cells (RBCs), a classification for RBCs was added as a fourth tissue type. Detailed steps on how to annotate tissue and build a tissue classifier is available within guidelines provided by Aperio Genie (https://cpb-us-w2.wpmucdn.com/voices.uchicago.edu/dist/1/3053/files/2021/06/MAN-0098-Rev-E.pdf) and Definiens (https://www.imperial.ac.uk/media/imperial-college/medicine/facilities/film/Definiens-Developer-User-Guide-XD-2.0.4.pdf).

2.4.3. Data analysis and external validation—Once classifiers were optimized, tissue analysis was performed according to manufacturer guidelines (see Section 2.4.2), and raw area estimates for each tissue type and glass were obtained from the program analysis output, a relative proportion of area for each tissue type was calculated for each mammary tissue section as follows:

To standardize tissue area across studies, the area of glass was subtracted from the manually selected analysis area for each tissue compartment. After subtracting non-tissue area within each section (e. g., glass), the proportion of epithelium, stroma and adipose were calculated as the area of each tissue type divided by the total tissue area for that specimen. For animals with two or more serial sections available, an area-weighted average was calculated across replicates.

External validation was performed by comparing pathologist-derived estimates of tissue area to the computationally derived estimates. Specifically, a pathologist blinded to the computational quantification estimated tissue compartment proportions for each dataset.

Agreement between the two estimates was assessed using Spearman correlation coefficients. Comparison of treatment groups for all three studies were performed using Welch's two sample t-tests or Kruskal Wallis rank sum tests followed by Dunn's multiple comparison test, using the Holm method to adjust for multiple comparisons [43–45]. All statistical analyses were performed in R version 4.0.3.

3. Results

We evaluated the ability of our digital histological analysis pipeline (Fig. 1) to accurately quantify tissue composition from three rodent mammary gland models across multiple reproductive windows and following relevant environmental exposures. Digital methods were compared against manual pathology review as the gold standard. We first investigated the effect of parity, a known mammary gland modifier [46], on the stromal tissue compartment of BALB/c mice from H&E- and Masson's trichrome-stained tissue sections (Fig. 2a). Stromal compartment quantification was highly concordant between manual pathology review and digital measurements (rho=0.89, $p < 0.0006$) (Fig. 2b). Consistent with manual review [19], stromal percentage quantified from H&E-stained tissue using our digital algorithm was significantly higher in parous mammary glands than in those from age-matched nulliparous females (Fig. 2c). Stromal area from Masson's Trichrome-stained tissue also showed a similar trend, with a higher proportion of stromal tissue in parous glands relative to those from nulliparous glands (Fig. 2d). Using our digital algorithm, we investigated the impact of BP-3 exposure on parity-induced stromal and epithelial modification. Interestingly, BP-3 exposure reversed the impact of parity on the stroma, as proportional stromal area was no longer elevated in glands from BP-3-treated parous mice relative to nulliparous (Fig. 3a). However, the effect of BP-3 was restricted to the stromal compartment, as epithelial proportional area remained significantly higher in both parous and parous+BP-3 glands relative to nulliparous glands (Fig. 3b).

Given that HFD has known impacts on the adiposity and development of the mammary gland [21], we sought to quantify stromal and adipose tissue in both LFD-fed and LFD-HFD-fed thirteen-week-old post-pubertal, *Trp53-null*-transplanted BALB/c mice, comparing digital and manual pathology review (Fig. 4a). The *Trp53-null* transplant model is an important environmental carcinogenesis model, and measurements by both our digital algorithm and manual review were strongly concordant for both stroma and adipose tissue (stroma rho=0.83, $p = 0.0031$; adipose tissue rho=0.84, $p = 0.0021$) (Fig. 4b, 4c). Using our digital pipeline, we found that LFD-HFD mice had a significantly decreased proportion of stromal area (Fig. 4d; p 0.0005), with a significantly increased proportion of adipose tissue area relative to LFD mice (Fig. 4e; p 0.0003). Similar to the impact of LFD-HFD exposure compared to LFD, BP-3 treatment influenced the impact of HFD on stromal and adipose tissue compartments, producing a nearly 2-fold reduction in the proportional percentage of stroma relative to HFD treatment alone, and a 7.5 % decrease relative to LFD mice (Fig. 5a; $p = 0.004$). Furthermore, HFD+BP3 treatment produced a 2-fold increase in the proportional percentage of adipose tissue area relative to HFD treatment alone, and an 8.2 % increase relative to LFD mice (Fig. 5b; $p = 0.008$).

Sprague-Dawley rats are a highly utilized and sensitive model for assessing toxicological insults in the mammary gland. H&E-stained tissue sections from prepubertally PFOA and zeranol-treated Sprague-Dawley female rats (Fig. 6a) were quantified. Comparison found that quantification of epithelial area by digital algorithm and manual pathology review were strongly correlated (Fig. 6b; rho = 0.83, $p < 0.001$). Based on the digital algorithm, PFOA zeranol exposure increased the median mammary gland epithelial area relative to vehicle controls by 1.4-fold, but these results were not statistically significant (p 0.09) (Fig. 6c).

A summary of all findings for each study and tissue compartment is available in Supplemental Table 1.

4. DISCUSSION

Mammographic breast density is among the strongest predictors of breast cancer risk [47]. Therefore, mammographic breast density provides a valuable tool to capture dynamic changes within breast tissue associated with risk of breast cancer. Mammographic density represents fibroglandular density due to both cellular and stromal components within the tissue. Recently, histologic density was shown to be associated with mammographic density [9]. In the studies reported herein, we applied digital imaging methodologies to examine histologic density in three rodent models and to validate their use to compare histologic mammary density in rodent models. Validation of digital analyses relied both on concordance with manual quantitation and concordance with well described biological effects associated with parity and high fat diet. Digital analysis confirmed an increase in the proportion of mammary stroma and epithelium as an outcome of parity, and similarly confirmed an increase in the proportion of mammary adipose tissue with a complementary decrease in the proportion of mammary stromal tissue with feeding a high saturated fat diet (HFD) at post-puberty. Digital analysis also showed good consistency between stromal and fibrous tissue measurements with H&E and Masson's trichrome, respectively. Thus, digital histology can be of utility across both staining methods. Furthermore, digital analysis performed well in both mouse and rat mammary tissues.

It is noteworthy that digital histologic analyses detected changes in mammary gland structure in response to toxicant exposures. BP-3 elicited a decrease in stromal area with no change in epithelial area in parous mice. In mice fed a continuous HFD, BP-3 also decreased the proportion of stroma, but at the same time increased the proportion of adipose tissue. Treatment of rats with a mixture of PFOA and zeranol elicited a trend toward increased epithelial area. These findings suggest that digital methodology holds promise for facile quantitation of relatively subtle toxicological effects in mammary tissue. Furthermore, the quantitative estimates presented in these preliminary studies could prove useful in power calculations to justify future rodent studies focused on histologic endpoints.

Differences in preparation protocols across laboratories often lead to significant variability in staining intensity and tissue analysis area, providing challenges in translating findings between rodent models and human clinical studies. However, the methods applied through our digital histological analysis pipeline help mitigate these challenges through careful selection of areas of analysis and use of appropriate unbiased software. Two digital analytic

platforms were used in the current studies, Definiens Tissue Studio and Aperio GENIE. Definiens performed better in the study examining dietary fat exposures, while Aperio GENIE performed better in the study examining nulliparous versus parous mice. There was more variability in staining intensity with the former tissue samples, while the latter were a more uniform set of samples. Aperio GENIE and Definiens are two commonly used tissue analysis software choices, but it is important to note that other software choices are publicly available, such as QuPath [48], ImageJ [49] and Fiji [50]. The uniformity of a sample set may dictate the best platform for analysis. Irrespective of the platform used, our analyses were comparable in detecting BP-3-related reduction in the proportion of stromal area and increase in the proportion of adipose tissue area.

While the focus of this study was methodological, the data obtained provide insight into alterations of rodent mammary structure induced by parity, HFD, BP-3, and PFOA plus zeranol. Parity induced increased stromal and fibrous tissue components in the mammary gland. Early parity is known to transiently increase breast cancer risk but confer long-term protection for human breast cancer [51], while breast density (and fibrous tissue) is a risk factor [52,53]. This underscores the complexity of age-dependent changes in the human breast. Thus, it is important to interpret histologic changes relative to key windows of susceptibility. Future studies should also evaluate whether parity influences the age-dependent involution of the rodent mammary gland, as this pattern would align with the early transient increase in risk. The positive association between parity and fibrous tissue observed here raises the question of whether parity and fibrous tissue will both heighten risk in rodent models, or whether one or the other will differ in rodent models from human observations of risk.

Mice with *Trp53-null* mammary glands fed HFD post-puberty showed increased proportional area of adipose tissue and decreased proportional area of stromal tissue compared to mice fed LFD. Similar, although less pronounced, changes were observed in mice fed continuously with HFD. Zhu et al. [24] showed that a post-pubertal HFD promoted *Trp53-null* tumorigenesis. Thus, at least in this dietary model that shows a decreased stromal compartment with HFD, increased mammary density may not be promotional. Obesity has been suggested to promote mammary tumorigenesis through increased interstitial fibrosis with thickening and increased stiffness of the extracellular matrix [54]. Our studies were carried out in BALB/c mice which are obesity resistant, but perhaps HFD increases stiffness of the extracellular matrix in the absence of increased thickness. Of course, the current model may be specific to *Trp53-null* tumorigenesis, where Trp53-null epithelium is embedded in wildtype stromal and adipose tissue, and/or changes in mammary density caused by diet. It should also be noted that these mice show increased adiposity with minimal weight gain.

Rats exposed to PFOA plus zeranol in puberty showed a modest trend toward an increased proportion of epithelial area without alteration of other glandular components demonstrating the utility of digital analysis in quantitation across all major tissue compartments. When PFOA plus zeranol-treated rats are subjected to a dimethylbenzanthracene (DMBA) mammary mutagenesis protocol, both latency of mammary tumors and tumor-free survival were decreased [33]. This suggests potential impacts on mammary tumorigenesis

through expansion of the epithelial compartment. Further examination of these important environmental toxicants in larger populations and across additional life stages will be needed to fully understand risk associated with PFOA and zeranol exposure.

In both wild-type parous mice and in nulliparous mice with *Trp53-null* mammary glands continuously fed HFD, BP-3 exposure reduced the proportional area of the mammary stroma. In the parous mice, there was no accompanying change in proportional epithelial area, while, in the mice fed HFD, there was an increased proportion of adipose tissue. The increase in adipose tissue in mice fed HFD is likely a direct result of the HFD containing 60 % kcal from fat versus the diet of the parous mice containing about 17 % kcal from fat. Parous mice with BP-3 exposure show modest decreases in tumor latency in a *Trp53-null* transplant model of mammary tumorigenesis (Vandenberg and Jerry, unpublished). While the effects of BP-3 on *Trp53-null* tumorigenesis were not tested in mice fed HFD continuously, mice fed post-pubertal HFD and treated with BP-3 showed enhanced *Trp53-null* tumorigenesis compared to mice not treated with BP-3 [26]. The potential role of decreased stroma in *Trp53-null* tumorigenesis needs to be further explored.

In the context of alteration of stroma by a toxicant, in utero DDT exposure has been correlated with breast cancer risk and increased breast density in daughters [55]. It would be interesting to use digital histological density in a rodent model to address these same issues, comparing cancer risk and mammary density with *in utero* DDT exposure. Such experiments might yield insight into the translation of digital histological density across humans and rodents. Certainly, the relationships between histologic density and cancer risk will require further investigation.

A strength of our study was the utilization of multiple rodent breast cancer models from separate laboratories that span different species, exposure windows, and staining methods. This approach allowed us to demonstrate the utility and robustness of our digital histological analysis pipeline. However, sample sizes from each study were small, and future work will be needed to validate the biological relationships observed herein. Our method for standardizing digital tissue analysis area, which includes both careful tissue selection and exclusion of non-tissue components, such as glass and artifacts, likely contributed to our ability to reveal biological relationships despite a small sample size, and may contribute to more reproducible findings across laboratories. We note that this analysis was done using software that is not freely available. However, similar approaches are available (e.g., QPath, Image J), and others have demonstrated the utility of these programs [48–50]. A limitation of our analysis is that we did not undertake comparison to free software approaches, and future work should consider the capabilities of any software for a given set of slides. Nevertheless, the histological analysis pipeline described herein could be used to better understand the role of various endocrine disrupting chemicals in modulating tissue composition as a biologically plausible pathway to increased cancer risk.

These digital histological studies identified effects of parity, HFD, and BP-3 exposure to reduce the proportion of stromal area in the murine mammary gland. Chollet-Hinton et al. [9] found that stroma is a strong modifier of the effects of aging on epithelial involution in the human breast. The robust effects of multiple factors on murine mammary stroma suggest

that such models may be useful in understanding the role of stroma in modulating the epithelial compartment in both healthy and cancerous mammary glands. The environment-mediated alterations in mammary stroma evident in these studies suggests that histology merits future focus in mammary gland biology, ideally through a variety of rodent models and with well-powered sample sizes. Digital histologic methods allow comparison across rodent models and between rodents and humans.

Supplementary Material

Refer to Web version on PubMed Central for supplementary material.

Acknowledgements

This work was supported by a National Institutes of Health (NIH), United States of America (USA) award of F31CA257388 to AMH, Breast Cancer and the Environment Research Program (BCERP) Grants from the National Institute of Environmental Health Sciences (NIEHS) and the National Cancer Institute (NCI), NIH, USA U01ES026119 to RCS and SZH, U01ES026140 to LNV, SSS and DJJ, University of Wisconsin – Madison Funding Award Agreement 713K053 to RCS and SZH associated with U01ES026127, and U01ES026130 to K. Michels (JS-P and YS). We thank University of North Carolina (UNC), USA, Pathology Service Core (PSC) for expert technical assistance. The UNC PSC is supported, in part, by grants from the NCI, USA (P30CA016086), NIH, USA (U54CA156733), NIEHS, USA (P30ES010126), University Cancer Research Fund (UCRF),USA, and North Carolina Biotechnology Center (NCBT), USA (2015-IDG-1007). The content is solely the responsibility of the authors and does not necessarily represent the official views of the National Institutes of Health.

Abbreviations:

BP-3	benzophenone-3
DMBA	dimethylbenzanthracene
H&E	hematoxylin and eosin
HFD	high fat diet
LFD	low fat diet
PFOA	perfluorooctanoic acid

References

[1]. Fenton SE, Endocrine-disrupting compounds and mammary gland development: early exposure and later life consequences, Endocrinol 147 (6 Suppl) (2006) S18–S24, 10.1210/en.2005-1131.

[2]. Wadia PR, Vandenberg LN, Schaeberle CM, Rubin BS, Sonnenschein C, Soto AM, Perinatal bisphenol A exposure increases estrogen sensitivity of the mammary gland in diverse mouse strains, Environ. Health Perspect 115 (2007) 592–598, 10.1289/ehp.9640. [PubMed: 17450229]

[3]. Stanko JP, Easterling MR, Fenton SE, Application of Sholl analysis to quantify changes in growth and development in rat mammary gland whole mounts, Reprod. Toxicol 54 (2015) 129–135, 10.1016/j.reprotox.2014.11.004. [PubMed: 25463529]

[4]. McGinley JN, Thompson HJ, Quantitative assessment of mammary gland density in rodents using digital image analysis, Biol. Proced. Online 13 (2011) 4, 10.1186/1480-9222-13-4. [PubMed: 21663682]

[5]. Degnim AC, Visscher DW, Berman HK, Frost MH, Sellers TA, Vierkant RA, Maloney SD, Pankratz VS, de Groen PC, Lingle WL, Ghosh K, Penheiter L, Tlsty T, Melton LJ 3rd, Reynolds

CA, Hartmann LC, Stratification of breast cancer risk in women with atypia: a Mayo cohort study, J. Clin. Oncol 25 (2007) 2671–2677, 10.1200/JCO.2006.09.0217. [PubMed: 17563394]

[6]. Tice JA, O'Meara ES, Weaver DL, Vachon C, Ballard-Barbash R, Kerlikowske K Benign breast disease, mammographic breast density, and the risk of breast cancer. J. Natl. Cancer Inst 105:1043–1049.

[7]. Kader T, Hill P, Rakha EA, Campbell IG, Gorringe KL, Atypical ductal hyperplasia: update on diagnosis, management, and molecular landscape, Breast Cancer Res 20 (2018) 39, 10.1186/s13058-018-0967-1. [PubMed: 29720211]

[8]. Sandhu R, Chollet-Hinton L, Kirk EL, Midkiff B, Troester MA, Digital histologic analysis reveals morphometric patterns of age-related involution in breast epithelium and stroma, Hum. Pathol 48 (2016) 60–68, 10.1016/j.humpath.2015.09.031. [PubMed: 26772400]

[9]. Chollet-Hinton L, Puvanesarajah S, Sandhu R, Kirk EL, Midkiff BR, Ghosh K, Brandt KR, Scott CG, Gierach GL, Sherman ME, Vachon CM, Troester MA, Stroma modifies relationships between risk factor exposure and age-related epithelial involution in benign breast, Mod. Pathol 31 (2018) 1085–1096, 10.1038/s41379-018-0033-7. [PubMed: 29463881]

[10]. Russo J, Moral R, Balogh GA, Mailo D, Russo IH, The protective role of pregnancy in breast cancer, Breast Cancer Res 7 (2005) 131–142, 10.1186/bcr1029. [PubMed: 15987443]

[11]. Albrektsen G, Heuch I, Hansen S, Kvåle G, Breast cancer risk by age at birth, time since birth and time intervals between births: exploring interaction effects, Br. J. Cancer 92 (2005) 167–175, 10.1038/sj.bjc.6602302. [PubMed: 15597097]

[12]. Chie WC, Huang CS, Chen JH, Chang KJ, Utility assessment for different clinical phases of breast cancer in Taiwan, J. Formos. Med. Assoc 99 (2000) 677–683. [PubMed: 11000729]

[13]. Russo J, Russo IH, Influence of differentiation and cell kinetics on the susceptibility of the rat mammary gland to carcinogenesis, Cancer Res 40 (1980) 2677–2687. [PubMed: 7388818]

[14]. Sivaraman L, Stephens LC, Markaverich BM, Clark JA, Krnacik S, Conneely OM, O'Malley BW, Medina D, Hormone-induced refractoriness to mammary carcinogenesis in Wistar-Furth rats, Carcinogenesis 19 (1998) 1573–1581, 10.1093/carcin/19.9.1573. [PubMed: 9771927]

[15]. Dunphy KA, Blackburn AC, Yan H, O'Connell LR, Jerry DJ, Estrogen and progesterone induce persistent increases in p53-dependent apoptosis and suppress mammary tumors in BALB/c-Trp53+/− mice, Breast Cancer Res 10 (2008) R43, 10.1186/bcr2094. [PubMed: 18471300]

[16]. Terry MB, Michels KB, Brody JG, Byrne C, Chen S, Jerry DJ, Malecki KMC, Martin MB, Miller RL, Neuhausen SL, Silk K, Trentham-Dietz A, Breast Cancer and the Environment Research Program (BCERP), Environmental exposures during windows of susceptibility for breast cancer: a framework for prevention research, Breast Cancer Res 21 (2019) 96, 10.1186/s13058-019-1168-2. [PubMed: 31429809]

[17]. Calafat AM, Wong LY, Ye X, Reidy JA, Needham LL, Concentrations of the sunscreen agent benzophenone-3 in residents of the United States: national health and nutrition examination survey 2003–2004, Environ. Health Perspect 116 (2008) 893–897, 10.1289/ehp.11269. [PubMed: 18629311]

[18]. Kim S, Choi K, Occurrences, toxicities, and ecological risks of benzophenone-3, a common component of organic sunscreen products: a mini-review, Environ. Int 70 (2014) 43–57, 10.1016/j.envint.2014.05.015.

[19]. LaPlante CD, Bansal R, Dunphy KA, Jerry DJ, Vandenberg LN, Oxybenzone alters mammary gland morphology in mice exposed during pregnancy and lactation, J. Endocr. Soc 2 (2018) 903–921, 10.1210/js.2018-00024. [PubMed: 30057971]

[20]. Matouskova K, Jerry DJ, Vandenberg LN, Exposure to low doses of oxybenzone during perinatal development alters mammary gland morphology in male and female mice, Reprod. Toxicol 92 (2020) 66–77, 10.1016/j.reprotox.2019.08.002. [PubMed: 31408669]

[21]. Olson LK, Tan Y, Zhao Y, Aupperlee MD, Haslam SZ, Pubertal exposure to high fat diet causes mouse strain-dependent alterations in mammary gland development and estrogen responsiveness, Int. J. Obes 34 (2010) 1415–1426, 10.1038/ijo.2010.51.

[22]. Zhao Y, Tan YS, Aupperlee MD, Langohr IM, Kirk EL, Troester MA, Schwartz RC, Haslam SZ, Pubertal high fat diet: effects on mammary cancer development, Breast Cancer Res 15 (2013) R100, 10.1186/bcr3561. [PubMed: 24156623]

[23]. Aupperlee MD, Zhao Y, Tan YS, Zhu Y, Langohr IM, Kirk EL, Pirone JR, Troester MA, Schwartz RC, Haslam SZ, Puberty-specific promotion of mammary tumorigenesis by a high animal fat diet, Breast Cancer Res 17 (2015) 138, 10.1186/s13058-015-0646-4. [PubMed: 26526858]

[24]. Zhu Y, Aupperlee MD, Zhao Y, Tan YS, Kirk EL, Sun X, Troester MA, Schwartz RC, Haslam SZ, Pubertal and adult windows of susceptibility to a high animal fat diet in Trp53-null mammary tumorigenesis, Oncotarget 7 (2016) 83409–83423, 10.18632/oncotarget.13112. [PubMed: 27825136]

[25]. Zhu Y, Aupperlee MD, Haslam SZ, Schwartz RC, Pubertally initiated high-fat diet promotes mammary tumorigenesis in obesity-prone FVB mice similarly to obesity-resistant BALB/c mice, Transl. Oncol 10 (2017) 928–935, 10.1016/j.tranon.2017.09.004. [PubMed: 29024822]

[26]. Kariagina A, Morozova E, Hoshyar R, Aupperlee MD, Borin MA, Haslam SZ, Schwartz RC, Benzophenone-3 promotion of mammary tumorigenesis is diet-dependent, Oncotarget 11 (2020) 4465–4478, 10.18632/oncotarget.27831. [PubMed: 33400736]

[27]. Zhao Y, Tan YS, Strynar MJ, Perez G, Haslam SZ, Yang C, Perfluorooctanoic acid effects on ovaries mediate its inhibition of peripubertal mammary gland development in Balb/c and C57Bl/6 mice, Reprod. Toxicol 33 (2012) 563–576, 10.1016/j.reprotox.2012.02.004.

[28]. White SS, Calafat AM, Kuklenyik Z, Villanueva L, Zehr RD, Helfant L, Strynar MJ, Lindstrom AB, Thibodeaux JR, Wood C, Fenton SE, Gestational PFOA exposure of mice is associated with altered mammary gland development in dams and female offspring, Toxicol. Sci 96 (2007) 133–144, 10.1093/toxsci/kfl177. [PubMed: 17132714]

[29]. White SS, Kato K, Jia LT, Basden BJ, Calafat AM, Hines EP, Stanko JP, Wolf CJ, Abbott BD, Fenton SE, Effects of perfluorooctanoic acid on mouse mammary gland development and differentiation resulting from cross-foster and restricted gestational exposures, Reprod. Toxicol 27 (2009) 289–298, 10.1016/j.reprotox.2008.11.054. [PubMed: 19095057]

[30]. White SS, Stanko JP, Kato K, Calafat AM, Hines EP, Fenton SE, Gestational and chronic low-dose PFOA exposures and mammary gland growth and differentiation in three generations of CD-1 mice, Environ. Health Perspect 119 (2011) 1070–1076, 10.1289/ehp.1002741. [PubMed: 21501981]

[31]. Roy JR, Chakraborty S, Chakraborty TR, Estrogen-like endocrine disrupting chemicals affecting puberty in humans–a review, Med. Sci. Monit 15 (2009) RA137–RA145. [PubMed: 19478717]

[32]. Yuri T, Nikaido Y, Shimano N, Uehara N, Shikata N, Tsubura A, Effects of prepubertal zeranol exposure on estrogen target organs and N-methyl-N-nitrosourea-induced mammary tumorigenesis in female Sprague-Dawley rats, Vivo 18 (2004) 755–761.

[33]. Su Y, Santucci-Pereira J, Dang NM, Kanefsky J, Rahulkannan V, Hillegass M, Joshi S, Gurdogan H, Chen Z, Bessonneau V, Rudel R, Ser-Dolansky J, Schneider SS, Russo J, Effects of pubertal exposure to butyl benzyl phthalate, perfluorooctanoic acid, and zeranol on mammary gland development and tumorigenesis in rats, Int. J. Mol. Sci 23 (2022) 1398, 10.3390/ijms23031398. [PubMed: 35163327]

[34]. Jerry DJ, Kittrell FS, Kuperwasser C, Laucirica R, Dickinson ES, Bonilla PJ, Butel JS, Medina D, A mammary-specific model demonstrates the role of the p53 tumor suppressor gene in tumor development, Oncogene 19 (2000) 1052–1058, 10.1038/sj.onc.1203270. [PubMed: 10713689]

[35]. Jovicic N, Jeftic I, Jovanovic I, Radosavljevic G, Arsenijevic N, Lukic ML, Pejnovic N, Differential immunometabolic phenotype in Th1 and Th2 dominant mouse strains in response to high-fat feeding, PLoS One 10 (2015), e0134089, 10.1371/journal.pone.0134089. [PubMed: 26218873]

[36]. Ip MM, Asch BB, Introduction: an histology atlas of the rodent mammary gland and human breast during normal postnatal development and in cancer, J. Mammary Gland Biol. Neoplasia 5 (2000) 117–118, 10.1023/a:1026435103940. [PubMed: 11149568]

[37]. Medina D, The mammary gland: a unique organ for the study of development and tumorigenesis, J. Mammary Gland Biol. Neoplasia 1 (1996) 5–19, 10.1007/BF02096299. [PubMed: 10887477]

[38]. Gonzalez H, Farbrot A, Larko O¨, A.-M. Wennberg, Percutaneous absorption of the sunscreen benzophenone-3 after repeated whole-body applications, with and without ultraviolet irradiation, Br. J. Dermatol 154 (2006) 337–340, 10.1111/j.1365-2133.2005.07007.x. [PubMed: 16433806]

[39]. Walpole SC, Prieto-Merino D, Edwards P, Cleland J, Stevens G, Roberts I, The weight of nations: an estimation of adult human biomass, BMC Public Health 12 (2012) 439, 10.1186/1471-2458-12-439. [PubMed: 22709383]

[40]. Ye X, Kuklenyik Z, Needham LL, Calafat AM, Automated on-line column-switching HPLC-MS/MS method with peak focusing for the determination of nine environmental phenols in urine, Anal. Chem 77 (2005) 5407–5413, 10.1021/ac050390d. [PubMed: 16097788]

[41]. Russo J, Gusterson BA, Rogers AE, Russo IH, Wellings SR, van Zwieten MJ, Comparative study of human and rat mammary tumorigenesis, Lab. Invest 62 (1990) 244–278. [PubMed: 2107367]

[42]. Russo J, Saby J, Isenberg WM, Russo IH, Pathogenesis of mammary carcinomas induced in rats by 7, 12-Dimethylbenz[a]anthracene, J. Natl. Cancer Inst 59 (1977) 435–445, 10.1093/jnci/59.2.435.

[43]. Dunn OJ, Multiple comparisons using rank sums, Technometrics 6 (1964) 241–252, 10.2307/1266041.

[44]. Holm S, A simple sequentially rejective multiple test procedure, Scand. J. Stat 6 (2) (1979) 65–70. http://www.jstor.org/stable/4615733.

[45]. Dinno Alexis. dunn.test: Dunn's Test of Multiple Comparisons Using Rank Sums. R package version 1.3.5 (2017). https://CRAN.R-project.org/packagedunn.test.

[46]. Russo J, Rivera R, Russo IH, Influence of age and parity on the development of the human breast, Breast Cancer Res. Treat 23 (1992) 211–218, 10.1007/BF01833517. [PubMed: 1463860]

[47]. Kerlikowske K, Ma L, Scott CG, Mahmoudzadeh AP, Jensen MR, Sprague BL, Henderson LM, Pankratz VS, Cummings SR, Miglioretti DL, Vachon CM, Shepherd JA, Combining quantitative and qualitative breast density measures to assess breast cancer risk, Breast Cancer Res 19 (2017) 97, 10.1186/s13058-017-0887-5. [PubMed: 28830497]

[48]. Bankhead P, Loughrey MB, Ferná JA, Dombrowski Y, McArt DG, Dunne PD, McQuaid S, Gray RT, Murray LJ, Coleman HG, James JA, Salto-Tellez M, Hamilton PW, QuPath: Open source software for digital pathology image analysis, Sci. Rep 7 (2017) 16878, 10.1038/s41598-017-17204-5. [PubMed: 29203879]

[49]. Schneider CA, Rasband WS, Eliceiri KW, NIH Image to ImageJ: 25 years of image analysis, Nat. Methods 9 (2012) 671–675, 10.1038/nmeth.2089. [PubMed: 22930834]

[50]. Schindelin J, Arganda-Carreras I, Frise E, Kaynig V, Longair M, Pietzsch T, Preibisch S, Rueden C, Saalfeld S, Schmid B, Tinevez JY, White DJ, Hartenstein V, Eliceiri K, Tomancak P, Cardona A, Fiji: an open-source platform for biological-image analysis, Nat. Methods 9 (2012) 676–682. [PubMed: 22743772]

[51]. Hsieh C, Pavia M, Lambe M, Lan SJ, Colditz GA, Ekbom A, Adami HO, Trichopoulos D, Willett WC, Dual effect of parity on breast cancer risk, Eur. J. Cancer 30 (2004) 969–973, 10.1016/0959-8049(94)90125-2.

[52]. Boyd NF, Guo H, Martin LJ, Sun L, Stone J, Fishell E, Jong RA, Hislop G, Chiarelli A, Minkin S, Yaffe MJ, Mammographic density and the risk and detection of breast cancer, N.Engl. J. Med 356 (2007) 227–236, 10.1056/NEJMoa062790. [PubMed: 17229950]

[53]. Yaghjyan L, Colditz GA, Collins LC, Schnitt SJ, Rosner B, Vachon C, Tamimi RM, Mammographic breast density and subsequent risk of breast cancer in postmenopausal women according to tumor characteristics, J. Natl. Cancer Ins 103 (2011) 1179–1189, 10.1093/jnci/djr225.

[54]. Seo BR, Bhardwaj P, Choi S, Gonzalez J, Andresen Eguiluz RC, Wang K, Mohanan S, Morris PG, Du B, Zhou XK, Vahdat LT, Verma A, Elemento O, Hudis CA, Williams RM, Gourdon D, Dannenberg AJ, Fischbach C, Obesity-dependent changes in interstitial ECM mechanics promote breast tumorigenesis, Sci. Transl. Med 7 (2015) 301ra130, 10.1126/scitranslmed.3010467.

[55]. Krigbaum NY, Cirillo PM, Flom JD, McDonald JA, Terry MB, Cohn BA, In utero DDT exposure and breast density before age 50, Reprod. Toxicol 92 (2020) 85–90, 10.1016/j.reprotox.2019.11.002. [PubMed: 31711904]

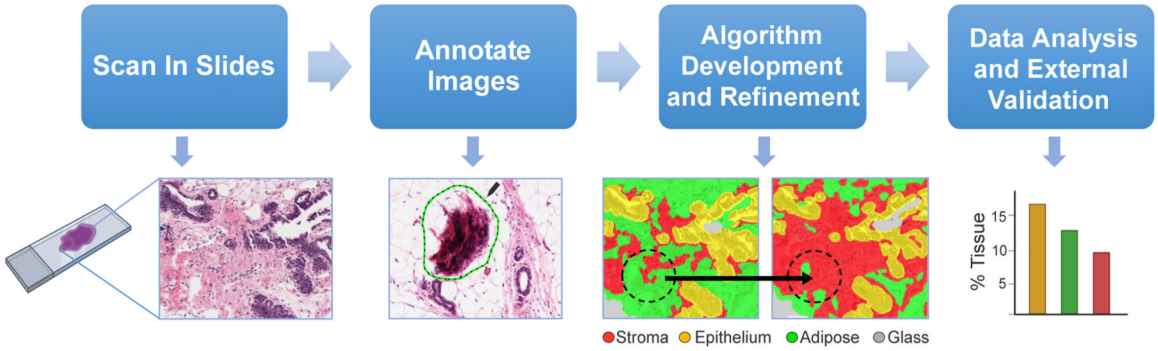

Fig. 1.

Flowchart of digital histologic analysis pipeline. Stained slides were first scanned into high-resolution digital images using a slide scanner and then manually annotated to remove large artifacts (illustrated by green dotted line). An algorithm was then developed using digital histology analysis software, such as Definiens and Aperio GENIE, to classify histological features based on variations in morphology, color, patterns, and texture. To develop the algorithm, we provided training data by manually selecting regions of interest (e.g., selecting representative examples of tissue compartments like epithelium, stroma, adipose and glass as shown above, or in the case of a specialized stain, selecting specific colors as “positive” and “negative”). Iterative improvements were then made based on these training pixels before being externally validated against manual quantification by a pathologist. Once validated, the data was analyzed for the biology of interest. A detailed description of this pipeline is described in Methods, Section 2.4.

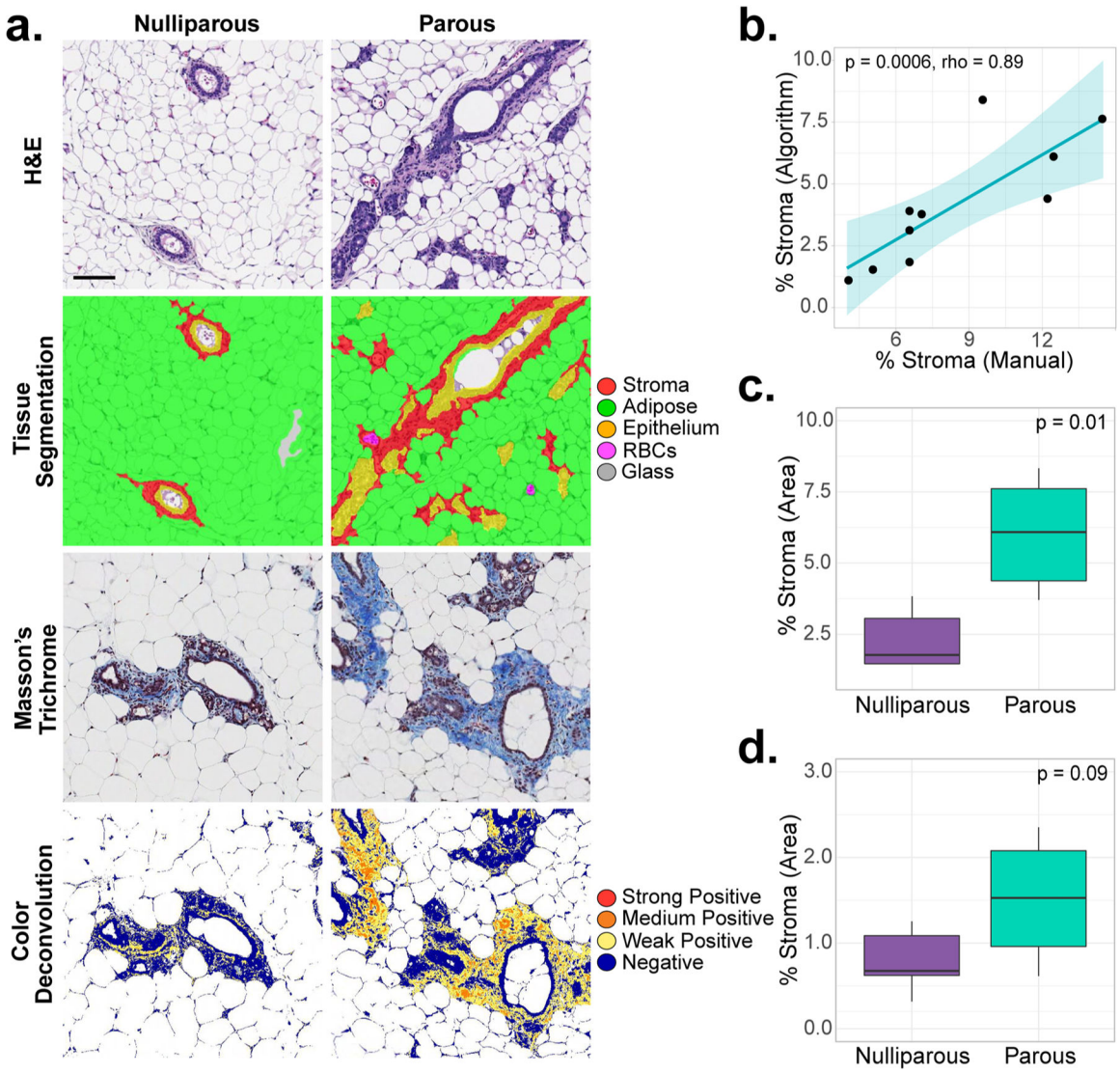

Fig. 2.

Quantification of stromal tissue in nulliparous and parous mice. (a) Representative images of H&E and Masson's Trichrome-stained mammary glands from nulliparous and parous mice, with overlays of digital tissue segmentation and color deconvolution. (b) Scatterplot displaying correlation between manual quantification (X-axis) and algorithm quantification (Y-axis) of percent stroma in tissue from H&E-stained mammary glands (Spearman's rho=0.89, p = 0.0006). Regression line and 95 % confidence intervals shown in blue. (c) Algorithm-based quantification of percent stroma in H&E-stained mammary glands from nulliparous and parous mice (p = 0.01). (d) Algorithm-based quantification of percent of stromal tissue in Masson's Trichrome-stained mammary glands from nulliparous and parous mice (p = 0.09). Scatterplot p-value and rho determined from a Spearman correlation test. Boxplot p-values determined from Welch's t-tests. Nulliparous: N = 5, Parous: N = 5; Scale bar: 100 μm.

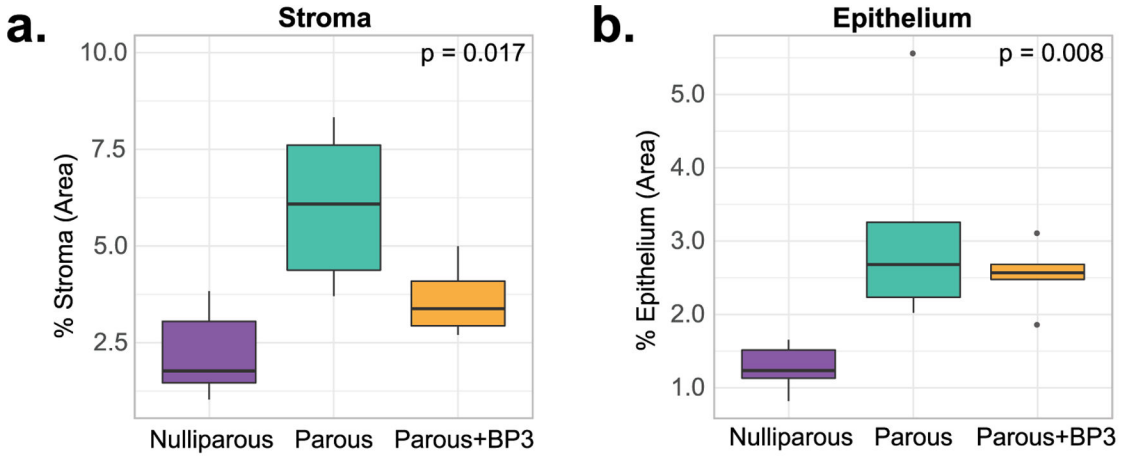

Treatment Group	% Stroma ± SD	Change in % Stroma	P-Value
Nulliparous	2.2 ± 1.2	Ref	Ref
Parous	6 ± 2	3.8	0.01
Parous+BP3	3.6 ± 0.9	1.4	0.23

Treatment Group	% Epithelium ± SD	Change in % Epithelium	P Value
Nulliparous	1.3 ± 0.3	Ref	Ref
Parous	3.2 ± 1.4	1.9	0.01
Parous+BP3	2.5 ± 0.4	1.2	0.03

Fig. 3.

Effect of Benzophenone-3 (BP-3) exposure on stromal and epithelial mammary tissue in parous mice. (a, upper panel) Boxplots displaying algorithm-based quantification of percent stroma in nulliparous, parous and BP3-treated parous mice (p = 0.017). (a, lower panel) Table displaying mean percent stroma ± standard deviation and change in percent stroma shown relative to nulliparous (parous: 3.8 %, p = 0.01; parous+BP3: 1.4 %, p = 0.23). (b, upper panel) Boxplots displaying algorithm-based quantification of percent epithelium in nulliparous, parous and BP3-treated parous mice (p = 0.008). (b, lower panel) Table displaying mean percent epithelium ± standard deviation and change in percent epithelium shown relative to nulliparous (parous: 1.9 %, p = 0.01; parous+BP3: 1.2 %, p = 0.03). P-values determined using the Kruskal-Wallis rank sum test with Dunn's multiple comparison test and adjusted using the Holm method. Kruskal-Wallis p-values comparing all experimental groups are displayed in upper panels; Dunn's multiple comparison test p-values displayed within lower panel tables. All boxplots display the median, interquartile range, minimum and maximum values for each group. Nulliparous: N = 5; Parous: N = 5; Parous+BP3: N = 5.".

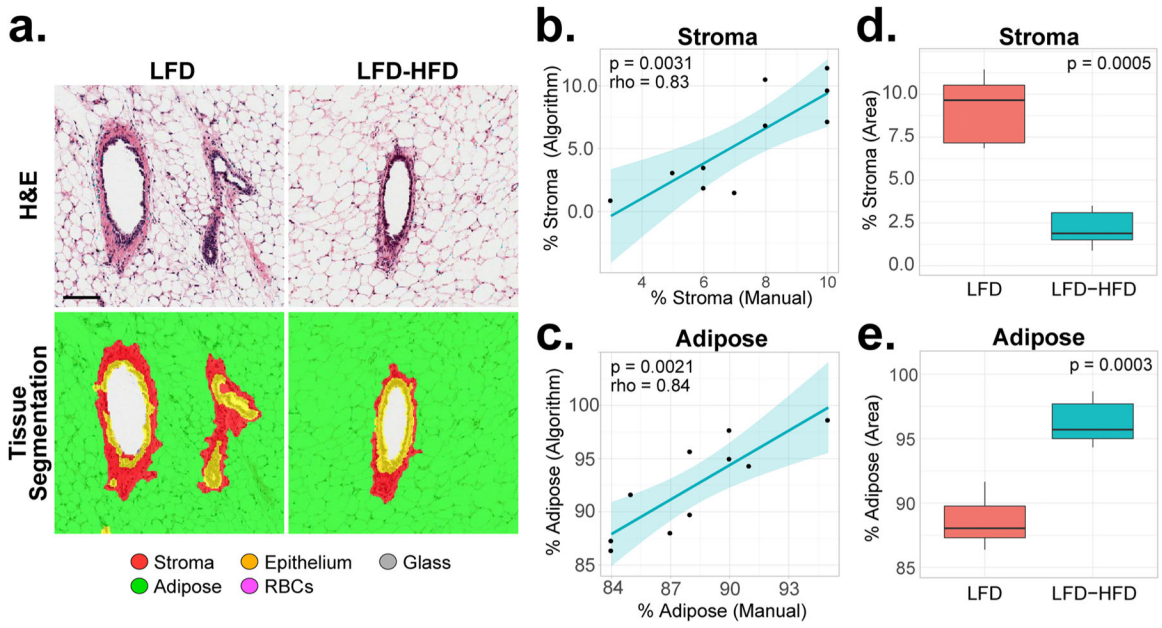

Fig. 4.

Quantification of stromal and adipose tissue in female 13-week-old post-pubertal *Trp53-null*-transplanted mice fed low and high fat diets. (a) Representative images of H&E-stained mammary glands from mice fed a low fat diet (LFD) or low fat followed by high fat diet (LFD-HFD), with overlays of digital tissue segmentation. (b-c) Scatterplots displaying correlation between manual quantification (X-axis) and algorithm quantification (Y-axis) of (B) percent stroma in tissue (Spearman's rho=0.83, p = 0.0031), and (c) percent adipose in tissue (Spearman's rho=0.84, p = 0.0021). Regression lines and 95 % confidence intervals shown in blue. (d) Algorithm-based quantification of percent stroma in mammary glands from LFD and LFD-HFD mice (p = 0.0005). (e) Algorithm-based quantification of percent adipose tissue in mammary glands from LFD and LFD-HFD mice (p = 0.0003). Scatterplot p-values and rho determined from Spearman correlation tests. Boxplot p-values determined from Welch's t-tests. LFD: N = 5, LFD-HFD: N = 5; Scale bar: 100 μm.

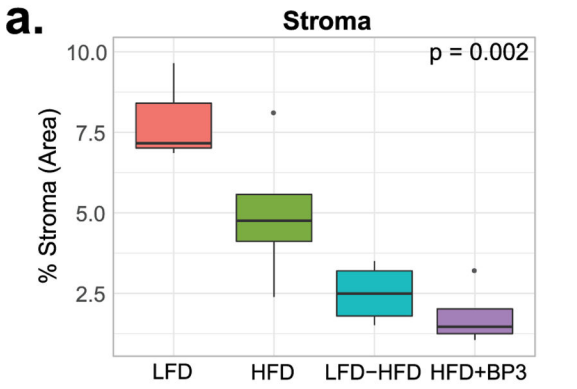

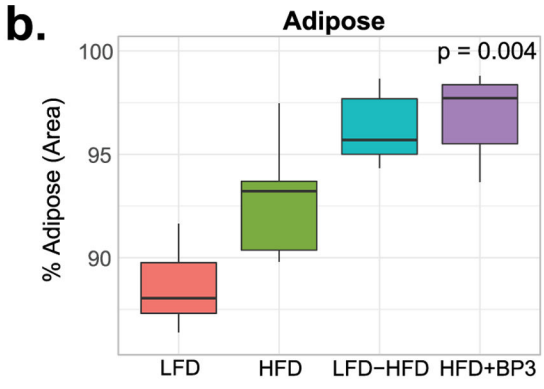

Treatment Group	% Stroma ± SD	Change in % Stroma	P-Value
LFD	9.1 ± 2	Ref	Ref
HFD	5 ± 2.1	-4.1	0.39
LFD-HFD	2.2 ± 1.1	-6.9	0.02
HFD+BP3	1.6 ± 0.9	-7.5	0.004

Treatment Group	% Adipose ± SD	Change in % Adipose	P-Value
LFD	88.6 ± 2	Ref	Ref
HFD	92.9 ± 2.1	4.3	0.3
LFD-HFD	96.3 ± 1.1	7.6	0.02
HFD+BP3	96.8 ± 0.9	8.2	0.008

Fig. 5.

Effect of BP-3 exposure on stromal and adipose mammary tissue in high fat diet-fed female pubertal mice. (a, upper panel) Boxplots displaying algorithm-based quantification of percent stroma in LFD, HFD, LFD-HFD, and HFD+BP3 treated mice (p = 0.002). (a, lower panel) Table displaying mean percent stroma ± standard deviation and change in percent stroma shown relative to LFD group (HFD: −4.1 %, p = 0.39; LFD-HFD: −6.9 %, p = 0.02; HFD+BP3: −7.5 %, p = 0.004). (b, upper panel) Boxplots displaying algorithm-based quantification of percent adipose in LFD, HFD, LFD-HFD, and HFD+BP3 treated mice (p = 0.004). (b, lower panel) Table displaying mean percent adipose ± standard deviation and change in percent adipose shown relative to LFD group (HFD: 4.3 %, p = 0.3; LFD-HFD: 7.6 %, p = 0.02; HFD+BP3: 8.2 %, p = 0.008). P-values determined using the Kruskal-Wallis rank sum test with Dunn's multiple comparison test and adjusted using the holm method. Kruskal-Wallis p-values comparing all experimental groups are displayed in upper panels; Dunn's multiple comparison test p-values displayed within lower panel tables. All boxplots display the median, interquartile range, minimum and maximum values for each group. LFD: N = 5; HFD: N = 5; LFD-HFD: N = 5; HFD+BP3: N = 5.

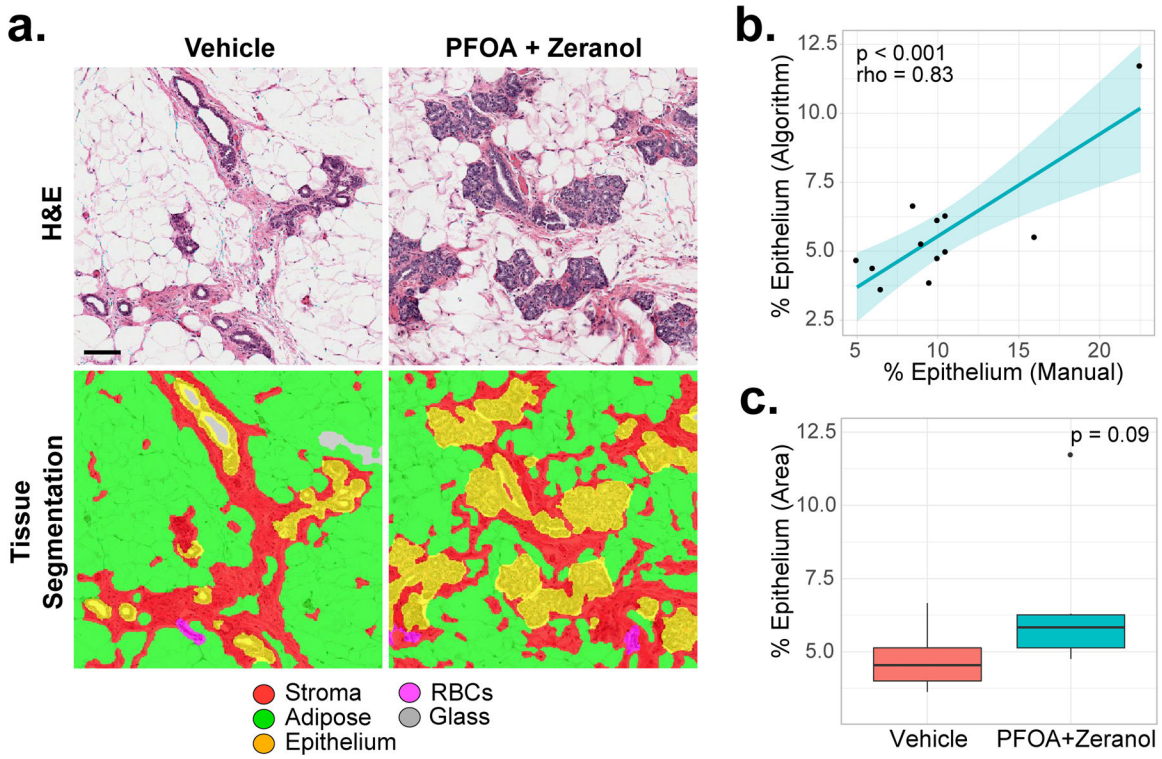

Fig. 6.

Effect of prepubertal PFOA and Zeranol exposure on epithelial mammary tissue in adult rats. (a) Representative images of H&E-stained mammary glands from PFOA+Zeranol and vehicle-treated Sprague-Dawley rats, with overlays of digital tissue segmentation. (b) Scatterplot displaying correlation between manual quantification (X-axis) and algorithm quantification (Y-axis) of percent epithelium in tissue (spearman's rho=0.83, $p < 0.001$). Regression line and 95 % confidence intervals shown in blue. (c) Algorithm-based quantification of percent epithelium in mammary glands of PFOA+Zeranol and vehicle-treated rats ($p = 0.09$). Scatterplot p-values and rho determined from a Spearman correlation test. Boxplot p-values determined from Wilcoxon rank sum test. Vehicle: N = 6, PFOA+Zeranol: N = 6; Scale bar: 100 μm.